

Sampling-Induced Resonance in an Encoderless Vector-Controlled Induction Motor Drive

Li Ran, *Member, IEEE*, and Yong Liao

Abstract—This paper illustrates an effect of sampling in an encoderless vector-controlled induction motor drive with a digital controller. The analysis focuses on the speed observer and the speed control loop which is executed at discrete instants. It is shown that the estimated speed can fluctuate between samples in the speed loop and cause a sustained resonance via feedback. The shaft inertia is not available to smooth the ripple of the estimated speed and the associated resonance could adversely affect the inverter and machine. An analytical model is proposed to evaluate the risk of such a condition in the design and on-site adjustment of control gains. The requirement for a smoothing filter in the speed loop is identified.

Index Terms—Digital control, drives, induction motors, observers.

NOMENCLATURE

| | |
|------------|--|
| r_s | Stator resistance. |
| L_{ls} | Stator leakage inductance. |
| r_r | Rotor resistance. |
| L_{lr} | Rotor leakage inductance. |
| r_m | Core loss resistance. |
| L_m | Magnetizing inductance. |
| L_s | Stator self-inductance, $= L_m + L_{ls}$. |
| L_r | Rotor self-inductance, $= L_m + L_{lr}$. |
| σ | Leakage coefficient, $= 1 - L_m^2 / (L_s L_r)$. |
| Φ_r^* | Rotor reference flux linkage. |

I. INTRODUCTION

THERE is continuing effort to develop encoderless vector controlled induction motor drives. Several speed estimation algorithms based on the steady-state and dynamic characteristics of the machine have been commercially implemented [1], [2]. An encoderless arrangement increases the system robustness and reduces manufacturing cost. Some algorithms also reduce the sensitivity of flux orientation to rotor resistance as the error of slip calculation can be compensated by the estimated speed. Recent studies addressed challenges in the low-speed range where measurement noise is comparable to the motor voltage used for speed estimation [3]. In many previous studies, the controller was treated in the continuous time domain. This paper will illustrate an important effect of discrete sampling in a practical encoderless drive with a digital controller.

It is known that sampling can cause phase delay and aliasing depending on the signal frequency and sampling rate [4, pp. 63–68]. In motor drives, the speed loop usually has a low sampling rate. With an encoder of high resolution, the measured speed is smooth due to the shaft inertia; a relatively long sampling period is acceptable and low-pass filtering is not necessary. However, in an encoderless drive, speed feedback is obtained from a software observer that can have fast transient response. As a result, considerable ripple of the speed feedback may be observed between samples. It is possible for the dynamics of the observer to interact with the sampling action in the speed loop. Sometimes, a sustained resonance can be caused although the actual speed remains almost constant due to inertia. There are reported cases of drives having been damaged by excessive resonant current in the switching devices and electrolytic dc-link capacitors [5], [6].

This is related to, but different from the classic problems of aliasing and hidden oscillation in a digital control system [4, pp. 160–164]. The steady-state speed is ideally a dc and should not cause aliasing. Resonance can still occur, which will be sampled explicitly in the control loop. For reasons to be expanded, the problem is associated with stability due to speed feedback from an observer and the ripple in the signal to be sampled is only introduced by the sampling action itself. Design and setting of control gains during commissioning must avoid instability. This requires investigation into the mechanism giving rise to the sampling-induced resonance.

This paper presents test results to demonstrate the resonance which is briefly explained referring to a simple model. An analytical method is developed to estimate the risk of sampling-induced resonance in an encoderless vector controlled induction motor drive. In addition to the discrete speed control loop and observer, the method also includes the response of the motor which will affect the phenomenon through current control on the magnetization and torque axes. Further experiments are performed to verify the method which is used to predict the effects of control gains and a smoothing filter. Although the focus is on a specific speed observer, the analysis can be extended to other encoderless systems. It is shown that a constraint, which is unnecessary with an encoder, needs to be considered when developing and operating encoderless drives.

II. SYSTEM CONFIGURATION AND SAMPLING-INDUCED RESONANCE

Fig. 1 shows the simplified block diagram of an encoderless vector controlled induction motor drive; the reader is referred to [2] for a detailed explanation. According to the flux and speed demands, the controller produces voltage applied to the motor

Manuscript received March 15, 2002; revised June 24, 2003. Abstract published on the Internet January 14, 2004.

L. Ran is with the School of Engineering, University of Durham, Durham DH1 3LE, U.K. (e-mail: li.ran@durham.ac.uk).

Y. Liao is with the Department of Electrical Engineering, Chongqing University, Chongqing, 400044, China (e-mail: yongliao@cqu@cta.cq.cn).

Digital Object Identifier 10.1109/TIE.2004.825371

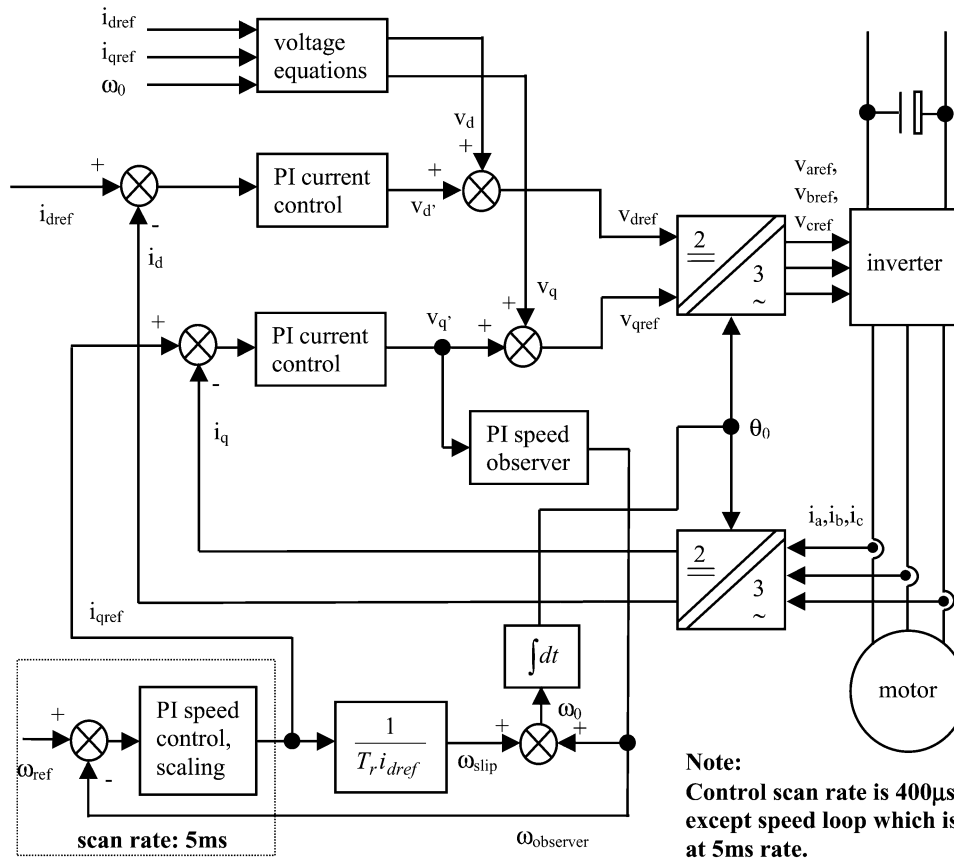


Fig. 1. Encoderless vector control of induction motor.

through an inverter. Components on the d (magnetization) and q (torque) axes consist of terms of the following voltage equations in the rotor flux reference frame. Outputs of the current controllers are added to them [7], [8]

$$\begin{cases} v_d = r_s i_{dref} - \omega_0 \sigma L_s i_{qref} \\ v_q = r_s i_{qref} + \omega_0 \sigma L_s i_{dref} + \omega_0 i_{dref} \frac{L_m^2}{L_r} \end{cases} \quad (1)$$

This is the voltage produced by the inverter and applied to the motor. The configuration shown in Fig. 1 is one of the typical systems with an encoderless arrangement.

The speed observer is driven by the output of the torque axis current controller. If the calculated slip and the above motor voltage are correct, the estimated speed will be the actual speed to give the correct supply frequency. Error in slip calculation, due to, e.g., inaccurate parameters, is reflected as a small error in the estimated speed. This paper is concerned with the particular speed observer while other estimation algorithms can be similarly analyzed [1], [2], [9]. The speed loop is scanned at a relatively slow rate, 5 ms, while the rest of the controller including the speed observer is executed every 400 μ s corresponding to the 2.5 kHz pulsewidth-modulation (PWM) process in the inverter. With respect to the sampling rate of the speed control loop, other parts can be regarded as continuous.

A test drive, whose parameters are detailed in the Appendix, is used to illustrate the phenomenon. The drive operates at 50% load and full speed. When the speed proportional gain is increased to 4 times of the given value, the q -axis current demand

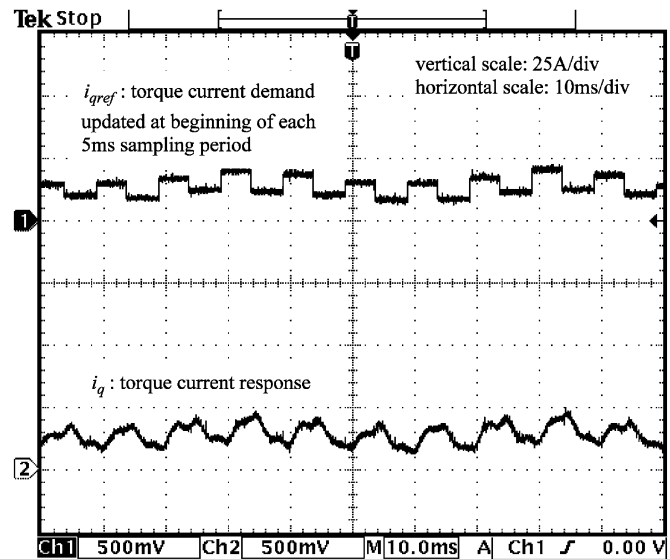


Fig. 2. Sampling-induced resonance in encoderless operation.

and feedback, i_{qref} and i_q , are shown in Fig. 2. They are measured by accessing the internal variables in the microprocessor system. Digital-to-analog conversion with appropriate scaling is used to plot these signals on the scope. The result shows resonance with a period of 10 ms, i.e., twice the sampling time of the speed loop. The demand remains constant between two sampling points. Since i_q is the torque producing or “active” current component, the resonance implies a pulsating air-gap torque and

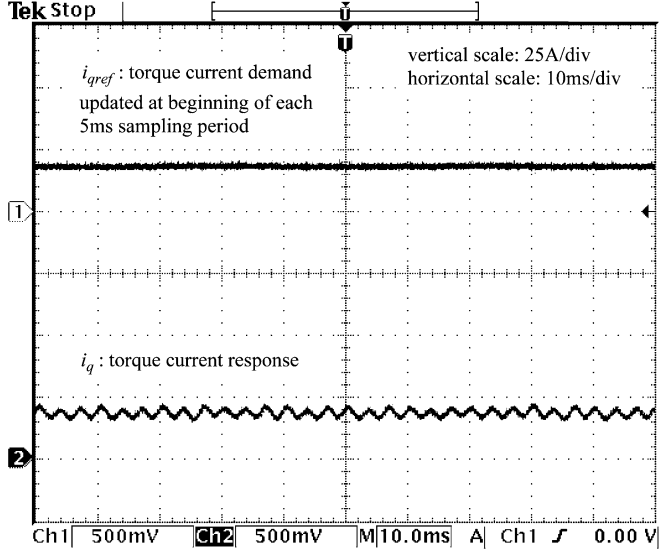


Fig. 3. Measurements in operation with encoder.

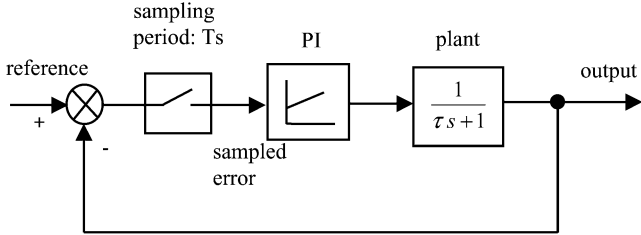


Fig. 4. A simple example system.

also an exchange of real power between the ac and dc sides of the inverter. Because of the latter, harmonic currents at 100 Hz and its integer multiples will flow through the dc link causing unexpected harmonics at the drive input side [10].

Fig. 3 shows the measurements under a comparative condition with speed feedback taken from a shaft encoder instead of the observer. The resonance disappears. The torque (q)-axis current only contains some sixth harmonic of 50 Hz due to internal compensation of the dc-link voltage ripple caused by the input diode rectifier. Therefore, the sampling-induced resonance on the q axis seems to be associated especially with the encoderless mode of the drive. It was checked that reference on the magnetization (d) axis is constant during resonance, suggesting the cause of the resonance is in the speed loop.

III. QUALITATIVE EXPLANATION

Fig. 4 shows a sampled system with digitized proportional–integral (PI) control. The plant to be controlled is first order and continuous. The digital PI controller is based on the sampled error and the control action is determined assuming that the error is constant in the entire sampling period.

To illustrate that sustained resonance can happen, assume that the output is already oscillating between samples as shown in Fig. 5. At time $t = t_1$, the output is at point “A.” The output is then sampled and the error, $e_1 = \Delta E/2$, is calculated. Since the error is positive, the controller will drive the output to increase. After a sampling period, the output reaches point “B” where it

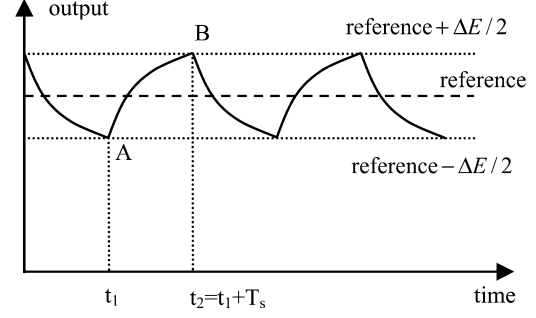


Fig. 5. Possible response of example system.

is sampled again. The error becomes $e_2 = -\Delta E/2$. As it is now negative, the controller forces the output to reduce. The resonance is sustained if the rise of the output in one sampling period equals the decrease in the next, as shown in the figure. At point “A” the discrete controller produces the following control action applied to the plant:

$$K_p \frac{\Delta E}{2} + K_i T_s \frac{\Delta E}{2} = \frac{\Delta E}{2} (K_p + K_i T_s) \quad (2)$$

where K_p and K_i are the proportional and integral gains, while T_s the sampling period. The solution for response in the time domain gives the following relationship for sustained resonance:

$$\frac{\Delta E}{2} (K_p + K_i T_s) (1 - e^{-T_s/\tau}) = \Delta E. \quad (3)$$

This further implies the condition below for $\Delta E > 0$

$$\frac{1}{2} (K_p + K_i T_s) (1 - e^{-T_s/\tau}) = 1. \quad (4)$$

It means that a digital controller does not provide strictly “closed-loop” control between samples. Assuming constant error in a period, control action is determined and applied at sampling instants. The response can have ripple between samples during which the system is not under “closed-loop” control. The ripple depends on the inertia or time constant of the plant. The analysis can be extended to show that the resonance increases and is unstable if $(K_p + K_i T_s)(1 - e^{-T_s/\tau})/2 > 1$, and is attenuated otherwise. In practice, unstable resonance can sustain due to limiting functions in the system [11]. In this example, sustained or unstable resonance is more likely if the sampling period is long or the time constant of the plant is short.

IV. MODELING OF THE ENCODERLESS DRIVE

In order to analyze the effect of sampling in the speed control loop which is executed every 5 ms, it is necessary to model the response of the estimated speed to a disturbance on i_{qref} produced by the discrete speed controller. Motor current response should be included in the model although the motor speed could be practically constant. The motor voltage equations (stator side) in the rotor flux orientated d – q axes are

$$\begin{cases} v_d = r_s i_d + \left(\frac{L_m^2}{L_r} + \sigma L_s \right) \frac{di_d}{dt} - \omega_0 \sigma L_s i_q \\ v_q = r_s i_q + \sigma L_s \frac{di_q}{dt} + \omega_0 \left(\frac{L_m^2}{L_r} + \sigma L_s \right) i_d. \end{cases} \quad (5)$$

The derivative terms are included because the short-circuit time constant of a large induction motor can be longer than 5 ms; steady state will not be reached within a sampling period [7]. In the Laplace domain, the incremental form of the motor equations is

$$\begin{bmatrix} \Delta V_d \\ \Delta V_q \end{bmatrix} = \begin{bmatrix} r_s + \left(\frac{L_m^2}{L_r} + \sigma L_s\right) s & -\omega_0 \sigma L_s & -\sigma L_s i_{q0} \\ \omega_0 \left(\frac{L_m^2}{L_r} + \sigma L_s\right) & r_s + \sigma L_s s & \left(\frac{L_m^2}{L_s} + \sigma L_s\right) i_{d0} \end{bmatrix} \times \begin{bmatrix} \Delta I_d \\ \Delta I_q \\ \Delta \Omega_0 \end{bmatrix} \quad (6)$$

where i_{d0} and i_{q0} are the average current on the d and q axes. ω_0 denotes the average supply frequency. s is the variable introduced by Laplace transform. The supply frequency is a variable rather than constant and, hence, $\Delta \Omega_0$ appears in (6); $\Delta \Omega_0$ is the Laplace transform of $\Delta \omega_0$ which is in the time domain. In the controller, the supply frequency is determined as the sum of the estimated rotor speed (converted to electrical) and the calculated slip frequency. Both of them are affected by the disturbance.

Corresponding to a disturbance in the torque current demand, Δi_{qref} , the change of motor voltage can be derived as follows including the response of current controllers. This is based on the actual controller configuration shown in Fig. 1 and further detailed by (1). See (7), shown at the bottom of the page, where K_p and K_i are the common proportional and integral gains of the current controllers. The calculated slip is proportional to the torque current demand, while the speed observer is driven by the output of the current controller on the torque axis. It is therefore possible to express the increments of supply frequency and estimated speed in terms of current

$$\Delta \Omega_0 = P_p \left(K_{p-ob} + \frac{K_{i-ob}}{s} \right) \left(K_p + \frac{K_i}{s} \right) \times (\Delta I_{qref} - \Delta I_q) + \frac{r_r}{\left(\frac{L_m^2}{L_r}\right)} \Delta I_{qref} \quad (8)$$

$$\Delta \Omega_{observer} = \left(K_{p-ob} + \frac{K_{i-ob}}{s} \right) \left(K_p + \frac{K_i}{s} \right) \times (\Delta I_{qref} - \Delta I_q) \quad (9)$$

where K_{p-ob} and K_{i-ob} are the proportional and integral gains of the observer, and P_p the number of pole pairs of the machine. $\Delta \Omega_{observer}$ is the Laplace transform of the change of the estimated mechanical speed.

Based on the above relationships, it is possible to derive a Laplace transfer function from the initial disturbance in the torque current demand, ΔI_{qref} , to the variation of estimated speed $\Delta \Omega_{observer}$. The result is complicated and unsuitable for further analysis. Alternatively, frequency response of $\Delta \Omega_{observer}(j\omega)/\Delta I_{qref}(j\omega)$ can be numerically computed. A

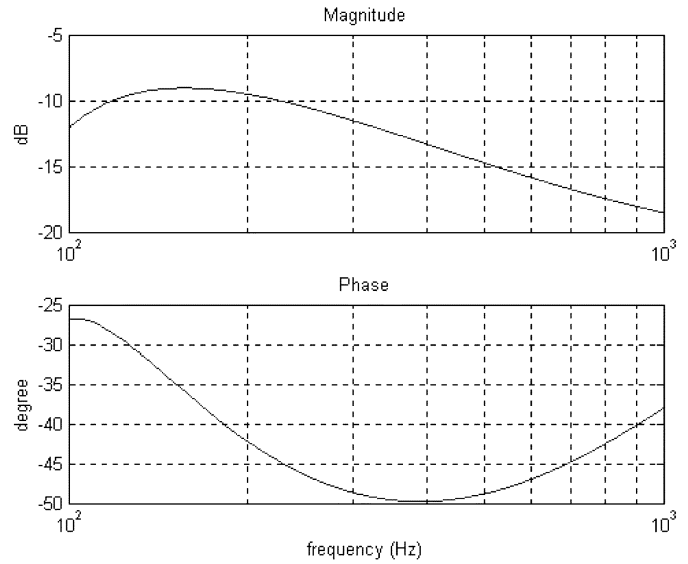


Fig. 6. Bode plots of frequency response $\Delta \Omega_{observer}(j\omega)/\Delta I_{qref}(j\omega)$.

simplified transfer function is then proposed to represent the system in the concerned frequency range [12, pp. 409–426].

Fig. 6 shows the Bode plots for the test system with the given settings, computed using the above relationships. The concerned frequency range is chosen to be from 100 to 1000 Hz, which covers the observed resonance and its harmonics up to the 10th. A first order transfer function is proposed to model the obtained response. Fig. 6 indicates that the phase delay is -45° at about 200 Hz. The amplitude is about constant (-10 dB) below 200 Hz. Therefore the corner frequency of the first-order system is chosen to be 200 Hz. As frequency increases, the amplitude decreases but the phase angle eventually stops decreasing instead of reaching -90° as in a first order system. Modeling the actual system using a first-order transfer function is, thus, a conservative representation exaggerating the phase delay. If the controller gains are determined to ensure the model to be stable, the practical system will always be stable. The transfer function that has the corner frequency and approximates the amplitude over the whole frequency range is

$$\frac{\Delta \Omega_{observer}}{\Delta I_{qref}} = \frac{0.56}{0.796 \times 10^{-3}s + 1}. \quad (10)$$

The first-order transfer function is suitable to derive explicitly the stability region for the speed control gains; as to be shown in the next section. In a more general case, it is suggested that a more complicated transfer function be used to “curve fit” the Bode plots obtained. The transfer function with known coefficients is then used in time-domain simulation to evaluate the risk of sampling-induced resonance in the speed loop. This method will also be briefly described in the next section using the test drive system as an example.

$$\begin{bmatrix} \Delta V_d \\ \Delta V_q \end{bmatrix} = \begin{bmatrix} -\left(K_p + \frac{K_i}{s}\right) & 0 & -\sigma L_s i_{q0} & -\omega_0 \sigma L_s \\ 0 & -\left(K_p + \frac{K_i}{s}\right) & \left(\sigma L_s + \frac{L_m^2}{L_r}\right) i_{q0} & K_p + \frac{K_i}{s} + r_s \end{bmatrix} \begin{bmatrix} \Delta I_d \\ \Delta I_q \\ \Delta \Omega_0 \\ \Delta I_{qref} \end{bmatrix} \quad (7)$$

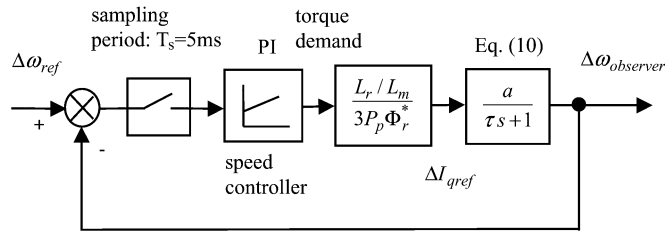


Fig. 7. Simplified speed control loop.

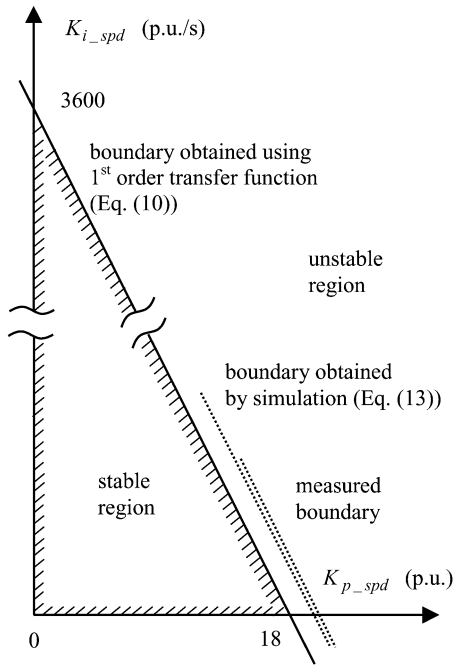
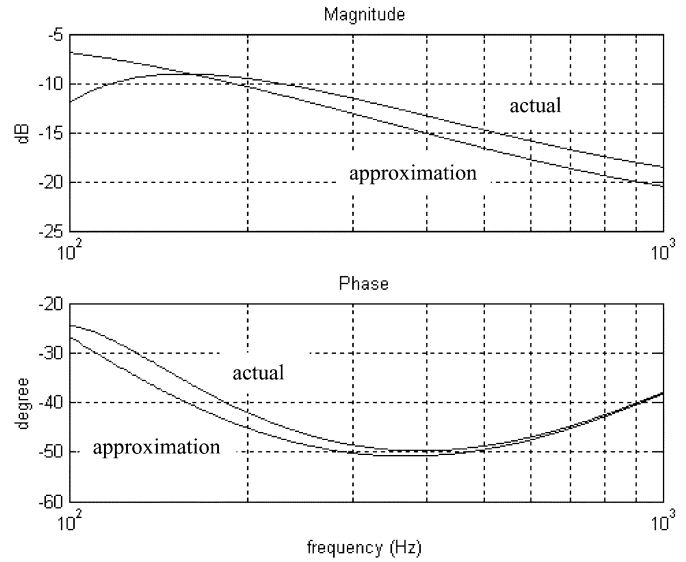


Fig. 8. Calculated stability region.

V. EVALUATION OF SAMPLING-INDUCED RESONANCE

With the derived transfer function, the discrete speed control loop of the encoderless drive system is reduced in Fig. 7. Output of the speed controller corresponds to the torque demand which is scaled to give the reference torque producing current. The scaling factor depends on rotor flux. The following results will therefore change as flux changes in field-weakening operation. The speed control loop consists of a discrete PI controller whose gains are expressed in per unit (p.u.). For the proportional gain K_{p_spd} , 1 p.u. means that the torque demand equals the motor rated torque for a speed error which is equal to the rated speed. Similarly, 1 p.u. of the integral gain K_{i_spd} produces such a torque demand if the speed error lasts for a second.

Theoretical analysis similar to that described in Section III can be performed in order to assess if sampling-induced resonance will occur for a given pair of gains of the speed controller. The calculated stability region of the gains is shown in Fig. 8. Within the region, the discrete speed control loop is stable and sampling-induced resonance is prevented. As a feature of the discrete PI controller, the proportional and integral gains have a similar effect in determining the control action at the beginning of a sampling period. Suppose the sampled speed error is $\Delta\omega$, the proportional term produces a control action according to $K_{p_spd}\Delta\omega$, while the contribution from the integral term is


 Fig. 9. Approximation of frequency response $\Delta\Omega_{observer}(j\omega)/\Delta I_{qref}(j\omega)$.

$K_{i_spd}T_s\Delta\omega$. Therefore, K_{p_spd} is equivalent to $K_{i_spd}T_s$. The boundary of the stability region is, thus, determined as

$$K_{p_spd} + K_{i_spd} \cdot T_s < \Theta \quad (11)$$

where Θ is a constant dependent on the dynamics of the system, which is approximated by the transfer function, and the sampling period. From (4) and the above explanation on p.u. gains,

$$\Theta = 2 \frac{3P_p\Phi_r^* \frac{L_m}{L_r}}{a \left(1 - e^{-\frac{T_s}{\tau}}\right)} \frac{\omega_{rate}}{T_{rate}} \quad (12)$$

For the test drive system, the value of Θ is calculated to be 17.6 p.u. which was used to plot the stability region shown in Fig. 8. The resonance shown earlier in Fig. 2 was captured with K_{p_spd} set to 20 p.u. and K_{i_spd} set to 100 p.u.. As far as the sampling-induced resonance is concerned, the overall effect of the speed control gains was $K_{p_spd} + K_{i_spd} \cdot T_s$, i.e. 20.5 p.u. for $T_s = 5$ ms. The gains were, thus, outside the stability region and the system was unstable.

The following transfer function can be used to better ‘‘curve fit’’ the frequency response shown in Fig. 6. The comparison of Bode plots is shown in Fig. 9. Higher order functions can be used to improve the agreement. The transfer function is used in a discrete time-domain simulation with progressively increased control gains. Unstable response is observed after $K_{p_spd} + K_{i_spd} \cdot T_s$ becomes greater than ~ 20 p.u.. Compared with the previous value of 17.6 p.u., the stability region is enlarged confirming that the first order representation previously used was indeed conservative. Fig. 8 also compares the stability region obtained using different models and measurement; second-order representation gives a closer result to the measurement

$$\frac{\Delta\Omega_{observer}}{\Delta I_{qref}} = \frac{6.46 \times 10^{-7}s^2 + 4.18 \times 10^{-13}s + 0.144}{9.68 \times 10^{-6}s^2 + 8.06 \times 10^{-3}s + 1} \quad (13)$$

Fig. 10 shows the time-domain measurement when the speed control gains are set so that $K_{p_spd} + K_{i_spd} \cdot T_s = 25$, clearly outside the stability region. The sampling-induced resonance is unstable. Compared with Fig. 2, the resonance is of

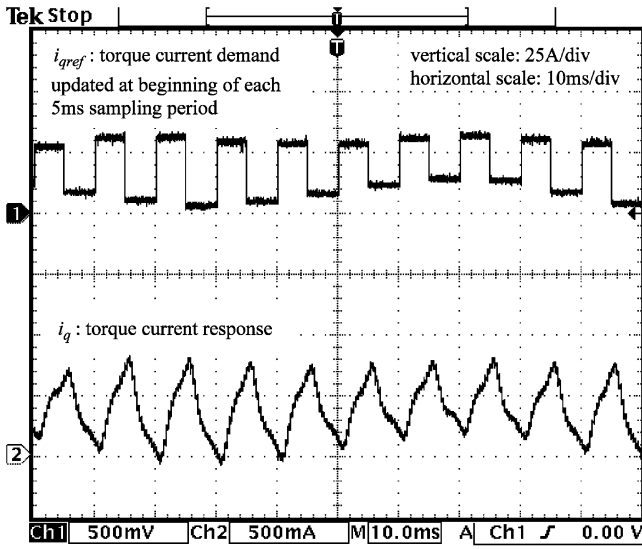


Fig. 10. Sustained resonance outside the stability region.

higher amplitude because the control action determined at the beginning of a sampling period is bigger for the same speed error. As the output torque demand of the speed controller is subject to internal limitation in the controller, the resonance sustains. The torque demand which is determined by the sampled speed error remains constant within a sample.

Note that for the same drive system, the derived transfer function is related to a particular operating point, and the gains in the current controller and speed observer. If the operating point and the gains have changed, the stability region for the speed loop should also be updated. Increasing the gains in the speed observer will generally increase the risk of sampling-induced resonance in the speed loop. As long as resonance is avoided, the gains can be optimized to improve the dynamic response [12, pp. 224–258].

VI. EFFECT OF A SMOOTHING FILTER

Extra smoothing filtering is not often used in drive systems for the speed feedback. However, the above analysis suggests that in encoderless operation, the estimated speed can contain significant ripple which is induced by the sampling process in the controller. It is, thus, expected that filtering added in the speed loop could attenuate the resonance and, hence, extend the stability region. Based on the first-order transfer function previously used to approximate the system response, analysis can be carried out to show the effect of a smoothing filter prior to sampling the estimated speed. The filter is supposed to be of first order with a time constant τ_f and unity dc gain. Then, the new stability limit can be obtained as given below

$$\Theta = \frac{2}{a} \frac{3P_p \Phi_r^* \frac{L_m}{L_r} \omega_{rate}}{1 + \frac{\tau}{(\tau_f - \tau)} e^{-\frac{T_s}{\tau}} - \frac{\tau_f}{(\tau_f - \tau)} e^{-\frac{T_s}{\tau_f}} \frac{T_{rate}}{T_{rate}}} \quad (14)$$

Fig. 11 plots this stability limit of $K_{p_spd} + K_{i_spd} \cdot T_s$ as a function of the filter time constant. Fig. 12 shows the measurement with $\tau_f = 5$ ms and $K_{p_spd} + K_{i_spd} \cdot T_s = 25$, i.e., outside the original but within the new stability region. The

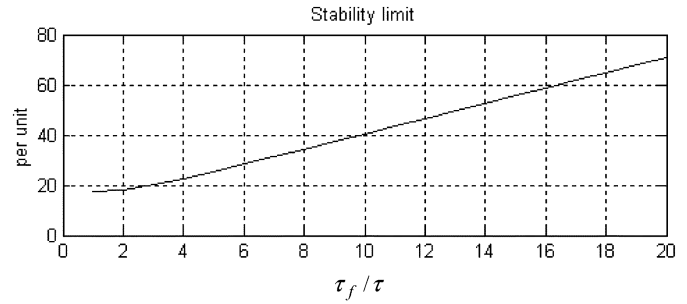


Fig. 11. Effect of smoothing filter.

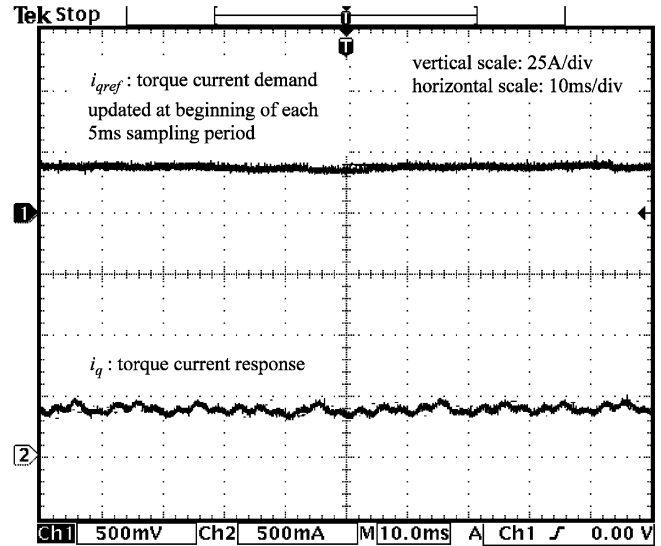


Fig. 12. Measurement with smoothing filter.

response is stable. Approximated in first order, the time constant of the system is $\tau = 0.796$ ms. The stability limit with the filter is $\Theta \approx 29$ according to Fig. 12 or (14); the smoothing filter has increased system stability. The effect of the smoothing filter agrees with a general rule in the design of digital control systems: the signal to be sampled should be limited in a bandwidth which is half of the sampling frequency [4, pp. 63–68]. The present study provides further insight regarding the practical application of such a rule: even the signal is expected to be smooth/constant, the sampling process itself can introduce ripple which can cause sustained resonance through feedback in the system.

In a drive system having an encoder, the shaft moment of inertia is inherently a low-pass filter to the speed signal. Therefore, no further filtering is required. The above analysis shows that an additional smoothing filter can be compulsory for an encoderless drive system and the stability region of the speed control gains depends greatly on the filter bandwidth.

This paper has analyzed one mechanism of sampling-induced resonance. It is believed that other mechanisms can also exist which will cause the same effect in an encoderless drive. For the test drive system used in this study, the response of the estimated speed $\Delta\omega_{observer}$ follows the change of the torque current demand Δi_{qref} in a way similar to a first-order system: if the torque current demand undergoes a sudden increase, the estimated speed will follow the increase due to the integrator. In

a general encoderless drive, the dynamics of the speed observer can be more complicated [9]. In some systems, there could exist the risk for the estimated speed to be sampled too soon at each time step, i.e., before the initial transient having decayed. The analysis presented in this paper can be extended to different situations.

VII. CONCLUSION

This paper has analyzed the sampling-induced resonance in an encoderless vector controlled induction motor drive. An analytical method was proposed to evaluate the risk of sustained resonance and predict the stability limit corresponding to the operating point and the settings of the internal current controller and speed observer. It is shown that, due to the “loss” of moment of inertia, resonance at half sampling frequency of the speed control loop can occur and an additional smoothing filter may be necessary for the speed feedback in the encoderless drive. The proposed method can be used to evaluate the stabilizing effect of the filter and help to determine the suitable proportional and integral gains in the speed controller.

It is expected that the study will help drive system designers and operators to recognize a special requirement of encoderless operation. This is particularly important for general drives which can be configured to operate in both encoder and encoderless modes.

APPENDIX
TEST SYSTEM PARAMETERS

Machine parameters:

| | |
|--------------|-------------------|
| voltage | 415 V, 50 Hz; |
| speed | 153.5 rad/s; |
| r_s | 0.168 Ω ; |
| r_m | 249 Ω ; |
| r_r | 0.1113 Ω ; |
| P_p | 2; |
| power | 22 kW; |
| rated torque | 143.3 N·m; |
| L_{ls} | 1.124 mH; |
| L_m | 42.5 mH; |
| L_{lr} | 1.931 mH; |
| stator | star connection. |

Current controller gains:

| | |
|-------|--------------|
| K_p | 3.0288 V/A; |
| K_i | 909 V/(A·s). |

Speed observer gains:

| | |
|-------------|-------------------|
| K_{p_ob} | 0.0277(rad/s)/V; |
| K_{i_ob} | 178(rad/s)/(V·s). |

Speed control gains (default values):

| | |
|--------------|----------|
| K_{p_spd} | 5 p.u.; |
| K_{i_spd} | 100 p.u. |

REFERENCES

- [1] G. M. Asher, “Sensorless estimation for vector controlled induction motor drives,” in *IEE Colloq. Vector Control Revisited*, London, U.K., 1998, pp. 6/1–6/5.
- [2] J. Holtz, “State of the art of controlled AC drives without speed sensor,” in *Proc. IEEE Int. Conf. Power Electronics and Drive Systems*, vol. I, Singapore, 1995, pp. 1–6.
- [3] Z. Beres and P. Vranka, “Sensorless IFOC of induction motor with current regulators in current reference frame,” *IEEE Trans. Ind. Applicat.*, vol. 37, pp. 1012–1018, July/Aug. 2001.
- [4] G. F. Franklin, J. D. Powell, and M. Workman, *Digital Control of Dynamic Systems*. Reading, MA: Addison-Wesley, 1998, pp. 63–68, 160–164.
- [5] D. Kastha and B. K. Bose, “Investigation of fault modes of voltage-fed inverter system for induction motor drive,” *IEEE Trans. Ind. Applicat.*, vol. 30, pp. 1028–1038, July/Aug. 1994.
- [6] P. Venet, F. Perisse, M. H. El-Husseini, and G. Rojat, “Realization of a smart electrolytic capacitor circuit,” *IEEE Ind. Applicat. Mag.*, vol. 8, pp. 16–20, Jan./Feb. 2002.
- [7] D. W. Novotny and T. A. Lipo, *Vector Control and Dynamics of AC Drives*. London, U.K.: Oxford Univ. Press, 1996, pp. 234–240.
- [8] M. Sumner and G. M. Asher, “Auto-commissioning for voltage-referenced voltage-fed vector-controlled induction motor drives,” *Proc. Inst. Elect. Eng.*, pt. B, vol. 140, no. 3, pp. 187–200, 1993.
- [9] P. Vas, *Sensorless Vector and Direct Torque Control*. Oxford, U.K.: Oxford Univ. Press, 1998, pp. 401–504.
- [10] K. S. Smith and L. Ran, “PWM drives: Voltage-type harmonic sources in power systems,” *Proc. IEE—Generation, Transmission, Distrib.*, vol. 145, no. 3, pp. 293–299, 1998.
- [11] Control Techniques plc., *Drives and Servos Yearbook*, pp. 141–146, 1990.
- [12] R. C. Dorf and R. H. Bishop, *Modern Control Systems*: Prentice Hall, 2001, pp. 409–426, 224–258.



Li Ran (M’98) was born in Sichuan, China, in 1963. He received the Ph.D. degree in electrical engineering from Chongqing University, Chongqing, China, in 1989.

He then spent three years as a Lecturer at Chongqing University. Between 1992–1999, he was a Research Fellow at the universities of Aberdeen, Nottingham, and Heriot-Watt in the U.K., where he was involved in research on marine and offshore electrical systems and industrial drives. In 1999, he became a Lecturer in power electronics at Northumbria University, U.K. He recently joined the University of Durham, Durham, U.K. His present research interest is the control and grid-integration of offshore renewable energy systems.

Dr. Ran received a Stanley Gray Award—Offshore Technology from the Institute of Marine Engineers in 1999.



Yong Liao was born in Chongqing, China, in 1964. He received the M.Eng. degree in electrical machinery and the Ph.D. degree in power system control from Chongqing University, Chongqing, China, in 1988 and 1997, respectively.

He is currently a Professor of Electrical Machinery and Apparatus at Chongqing University. His research interests include the control of doubly fed electrical machines as used in renewable energy systems, including wind and micro-hydro generators. In 1998, he participated in the Global Development Programme of Rockwell Automation, Milwaukee, WI. Between 2001–2002, he was a Visiting Professor at Northumbria University, U.K.